

Quantum transport in a driven disordered potential: onset of directed current and noise-induced current reversal

D. V. Makarov and L. E. Kon'kov

Laboratory of Nonlinear Dynamical Systems,
 V.I. Il'ichev Pacific Oceanological Institute of the Far-Eastern Branch of the Russian Academy of Sciences,
 43 Baltiyskaya St., 690041, Vladivostok, Russia

Received: date / Revised version: date

Abstract. We study motion of a quantum wavepacket in a one-dimensional potential with correlated disorder. Presence of long-range potential correlations allows for existence of localized and extended states simultaneously. Weak time-dependent perturbation in the form of a fluctuating plane wave is superimposed onto the potential. This model can be realized in experiments with optically trapped cold atoms. Time-dependent perturbation causes transitions between localized and extended states. Owing to violation of space-time symmetries, there arises atomic current which is codirectional with the wave-like perturbation. However, it is shown that the perturbation can drag atoms only within some limited time interval, and then the current changes its direction. Increasing of the perturbation bandwidth and/or amplitude results in decreasing of the time of current reversal. We argue that onset of the current reversal is associated with inhomogeneity of diffusion in the momentum space, that is, momentum states corresponding to atom flights in the opposite direction to the dragging have longer lifetimes and can accumulate population.

PACS. 05.60.Gg Quantum transport – 37.10.Jk Atoms in optical lattices – 63.20.kd Electron-phonon interactions – 73.21.Hb Quantum wires

1 Introduction

It is well known that cold atoms trapped in optical lattices can serve as an excellent quantum simulator of solid-state physics phenomena [1]. For example, creation of artificial magnetic fields in 2D lattices allow for studying quantum Hall effect with exceptionally strong magnetic fields [2, 3, 4, 5, 6] which are hardly realized in real solid-state experiments. Quantum ratchets with cold atoms [7, 8, 9, 10, 11, 12] can be considered from diverse viewpoints. For example, the atomic ratchets can serve as simulators of the related photogalvanic phenomena in solid-state nanostructures [13, 14, 15, 16, 17, 18, 19, 20, 21]. Besides, the ratchet effect has self-contained meaning as a tool for controllable transportation of atoms into some target region, that is of great importance in nanoscale technologies like quantum communication [22, 23].

From the viewpoint of various solid-state applications, it is reasonable to examine the possibility of gaining dc current if the spatially periodic potential is replaced by a random one. Indeed, it is well known that ballistic transport in 1D undriven disordered potentials is prevented by scattering processes which can give rise to the Anderson localization. However, external AC driving can significantly increase the localization length or lead to delocalization even within the tight-binding approximation [24, 25, 26] that doesn't take into account Landau-Zener inter-

band tunneling. As number of frequency components in the driving increases, the resulting transport transforms from subdiffusive to diffusive [27, 28, 29, 30, 31, 32, 33, 34]. Landau-Zener tunneling results in energy growth that also facilitates delocalization [35, 36]. So, one may expect that properly constructed external AC driving should give rise to directed ballistic current, i. e. the ratchet effect, provided certain time-space symmetries of the driving are violated. This is an important advantage of the ratchet effect as compared to the action of stationary directed forces: in the latter case eigenfunctions remain exponentially localized that infers the insulating regime.

In the present work, AC driving is superimposed onto smooth potential with correlated disorder. We consider AC driving being a superposition of two optical lattices whose amplitudes are small and subjected to broadband modulation that is modeled using harmonic noise. With proper choice of the phase shift between the modulating signals, the driving force becomes a running plane wave experiencing time and space fluctuations. This kind of ratchets is known as travelling potential ratchets and considered in [37, 38, 39, 40, 41, 42]. They can be used as a quantum simulator of electron-phonon interactions in semiconducting materials [43, 44, 45, 46]. This issue is of especial importance as a promising way of electronic transport control by means of the stimulated phonon emission via a SASER [47, 48]. Interest to the configuration we con-

sider is substantially supported by recent results of [49], where non-trivial dependence of current on the perturbation strength was found for a somewhat similar system.

The paper is organized as follows. In the next section we give detailed description of the model studied. In particular, we study spectral properties of the undriven system and point out the presence of the mobility edge in the energy space. Also, we introduce AC driving involving harmonic noise and describe its basic properties. Section 3 contains results of numerical simulation. These results are analyzed in section 4 in terms of kinetic approach. In section 5 we summarize the results and outline ways of further research.

2 Model description

2.1 Time-independent part

One-dimensional motion of an atomic wavepacket is governed by the Schrödinger equation

$$i\hbar \frac{\partial \Psi}{\partial t} = -\frac{\hbar^2}{2M} \frac{\partial^2 \Psi}{\partial x^2} + [U(x) + \varepsilon V(x, t)]\Psi, \quad (1)$$

where ε is a small parameter. Function $U(x)$ describes

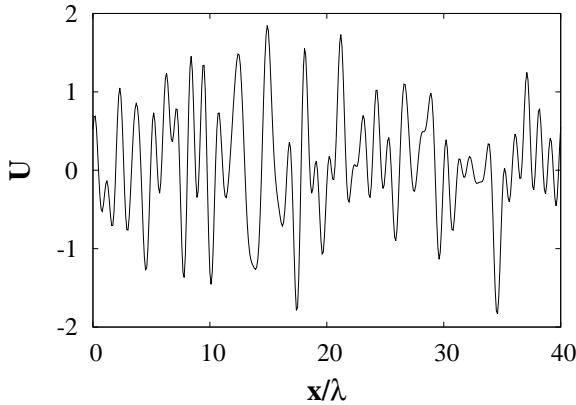


Fig. 1. A typical realization of potential $U(x)$, $\lambda = 2\pi/k_0$.

the time-independent part of the optical potential. We construct it as superposition of plane waves with random wavevectors and phases:

$$U = A\tilde{U}, \quad \tilde{U} = \sum_j \cos(k_0 x \cos \theta_j + \chi_j). \quad (2)$$

Here θ_j and χ_j are random phases with uniform distribution in the interval $[0 : 2\pi]$, and $k_0 = 1$. Coefficient A is determined by the normalization condition

$$A = \left(2 \langle \tilde{U}^2 \rangle_x\right)^{-1/2}, \quad (3)$$

where $\langle \dots \rangle_x$ denotes averaging over x . An example of $U(x)$ is presented in Fig. 1. According to the figure, $U(x)$ can

be regarded as some randomly-distorted lattice potential. It can serve as a model of an optical potential created by optical speckle pattern.

Autocorrelation function of the potential (2) obeys the following formula [50]

$$\langle U(x)U(x+d) \rangle \propto J_0(d), \quad (4)$$

where J_0 is the zero-order Bessel function of the first kind. Power-like asymptotics of J_0 implies the presence of long-range correlations. Long-range correlations result, according to [51], in the existence of the mobility edge, i. e. the energy boundary separating localized and delocalized states. A simple intuition suggests that the transition to the delocalization should occur with increasing energy. This transition should be reflected in the energy spectrum, in particular, in statistics of level spacings [52, 53, 54]

$$s = E_{n+1} - E_n, \quad (5)$$

where E_n and E_{n+1} are two consecutive energy values. In the insulating regime corresponding to the disorder-induced localization, eigenstates belonging to the same energy band don't substantially overlap in space, therefore, their energies are statistically independent and obey Poissonian distribution of level spacings

$$P(s) = \frac{1}{\langle s \rangle} \exp\left(-\frac{s}{\langle s \rangle}\right), \quad (6)$$

where $\langle s \rangle$ is the mean level spacing. Non-zero conductivity implies overlapping of eigenstates that gives rise to level repulsion and level spacing statistics is described by the Wigner surmise

$$P(s) = \frac{\pi}{2} \frac{s}{\langle s \rangle^2} \exp\left(-\frac{\pi s^2}{4 \langle s \rangle^2}\right). \quad (7)$$

Finally, in the regime of free motion that is not affected by the potential, energy spectrum inside a sample of length L with perfectly reflecting boundaries is described by simple formula

$$E_n = \frac{2\pi^2 \hbar^2}{L^2 m} n^2, \quad (8)$$

yielding

$$s_n = E_{n+1} - E_n \propto n. \quad (9)$$

This results in uniform distribution of level spacings. In the model we consider, this regime should be relevant for the range of high energy values.

Figure 2 demonstrates level spacing distributions corresponding to the different energy bands. Level spacing distributions were obtained by solving numerically the stationary Schrödinger equation with $\varepsilon = 0$ for a long sample ($L = 2000\pi$). In the lowest energy region, level distribution is well described by the Poissonian law (6), indicating localization of eigenstates. In the moderate energy region, $1 < E \leq 4$, level spacing distribution significantly deviates from the Poissonian form and is non-monotonous, revealing the presence of level repulsion. The high-energy

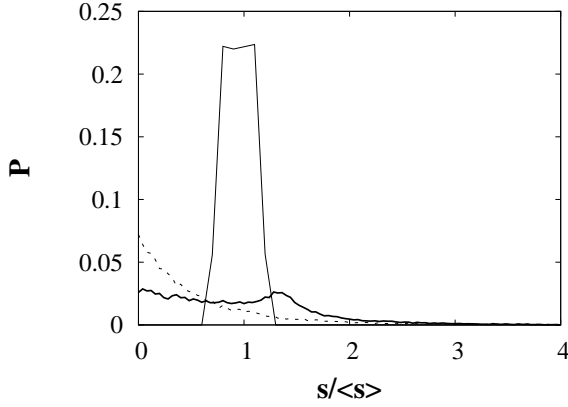


Fig. 2. Level spacing distributions in the energy bands corresponding to $E \leq 1$ (dashes), $1 < E \leq 4$ (thick solid), and $4 < E \leq 10$ (thin solid).

range represents step-like level spacing distribution consistent with (8). Indeed, formula (9) means that finite energy range corresponds to finite range of spacing values, with uniform spacing distribution inside this range. So, one can deduce the existence of the mobility edge in the range $1 < E \leq 4$, separating low-energy localized states and high-energy metallic ones.

2.2 Time-dependent perturbation

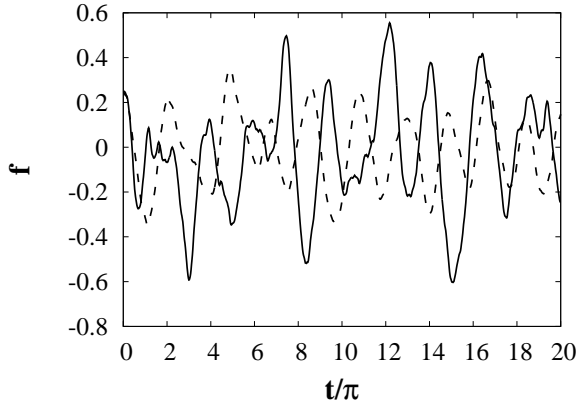


Fig. 3. Realizations of harmonic noise for $\Gamma = 0.1$ (dashes) and $\Gamma = 0.5$ (solid).

In the preceding section we had shown that, despite of the disorder, potential (2) simultaneously allows for localized and extended states, separated by the mobility edge. This gives rise to the possibility for transition between the insulating and conducting regimes by means of external time-oscillating driving. If the driving doesn't satisfy certain space-time symmetry relations, the resulting current can be directed [55]. Following [41,56], we use the perturbation $V(x, t)$ expressed as

$$V(x, t) = f(t) \sin x + f(t + \tau) \cos x, \quad (10)$$

where $f(t)$ is a broadband signal. Thus, $V(x, t)$ is given by superposition of two lattice potentials subjected to the amplitude modulation. Note that the modulating signal $f(t + \Delta)$ is the replica of the signal $f(t)$ with the time shift τ .

In experiments, broadband amplitude modulation of optical lattices can be realized using coherent frequency-modulated signals. However, in the present work we consider a more complicated case, when non-zero bandwidth of modulating signals is associated with uncontrollable stochastic processes. Nevertheless, it is assumed that the modulating signal can be recorded and reproduced. In particular, we model $f(t)$ as the so-called harmonic noise [57, 58]. Harmonic noise is described by coupled stochastic differential equations

$$\dot{f} = y, \quad \dot{y} = -\Gamma y - \omega_0^2 f + \sqrt{2\beta\Gamma}\xi(t), \quad (11)$$

where Γ is a positive constant, and $\xi(t)$ is Gaussian white noise. Realizations of harmonic noise can be calculated by means of mapping

$$\begin{aligned} f_{n+1} &= f_n + s_n h + \frac{1}{2}\alpha_n h^2 + \gamma Z_2(h), \\ s_{n+1} &= s_n + \alpha_n h + \gamma Z_1(h) - \frac{1}{2}\Gamma\alpha h^2 \\ &\quad + \Gamma\gamma Z_2(h) - \frac{1}{2}\Omega^2 s_n h^2, \end{aligned} \quad (12)$$

where h is the time step, $\alpha_n = -\Gamma s_n - \Omega^2 f_n$, $\gamma = \sqrt{2\beta\Gamma}$. Terms Z_1 and Z_2 are given by expressions

$$Z_1(h) = \sqrt{h}Y_1, \quad Z_2(h) = h^{3/2} \left(\frac{Y_1}{2} + \frac{Y_2}{2\sqrt{3}} \right), \quad (13)$$

where Y_1 and Y_2 are statistically independent Gaussian noises with unit variance. Realizations of harmonic noise with different values of Γ are exemplified in Fig. 3.

The terms $f(t)$ and $f(t + \tau)$ in (10) correspond to one and the same realization of harmonic noise and differ only by the temporal shift τ . The first two moments of harmonic noise are given by

$$\langle f \rangle = 0, \quad \langle f^2 \rangle = \frac{\beta}{\omega_0^2}. \quad (14)$$

We set $\beta = 1$, that is, the perturbation strength is solely determined by the parameter ε entering into (1). In the case of low values of Γ , the power spectrum of harmonic noise has the unique peak at the frequency

$$\omega_p = \sqrt{\omega_0^2 - \frac{\Gamma^2}{2}} \quad (15)$$

with the width

$$\Delta\omega = \sqrt{\omega_p + \Gamma\omega'} - \sqrt{\omega_p - \Gamma\omega'}, \quad (16)$$

where

$$\omega' = \sqrt{\omega_0^2 - \Gamma^2/4}.$$

One can easily find that

$$f(t) \rightarrow \sin(\omega_0 t + \phi_0),$$

as $\Gamma \rightarrow 0$. Setting $f(0) = 1$, $y(0) = 0$, and

$$\tau = \frac{\pi}{2\omega_0}, \quad (17)$$

one finds

$$V(x, t) = \sin(x - \omega_0 t) \quad (18)$$

in the case of $\Gamma = 0$. Hence, it turns out that $V(x, t)$ for $\Gamma > 0$ behaves as a fluctuating plane wave.

Owing to broken space-time symmetries [41], perturbation (10) can give rise to directed transport. In the semiclassical regime and in the case of the periodic potential $U(x)$, direction of the current coincides with the direction of the perturbation phase velocity [41], that is, the perturbation creates force that drags atoms towards $x \rightarrow \infty$. More intricate behaviour is observed in the deep quantum regime, when interband tunneling is negligible, and system dynamics is restricted to the lowest energy band. As it was shown in [49], current direction qualitatively depends on the perturbation amplitude. For low amplitude values, current velocity grows with increasing of the amplitude, until it becomes equal to the phase velocity of the perturbation. However, as the amplitude of the perturbation exceeds some threshold value, the current velocity rapidly decreases and changes its sign, that it, there appears transport in the opposite direction. This phenomenon is closely related to the specific form of Bloch oscillations. Addition of harmonic noise into the perturbation should, however, lead to interband transitions and thus violates the single-band picture of motion [59,60].

Taking into account some similarity between our model and the model considered in [49], it is reasonable to examine transport properties for different values of the perturbation amplitude ε . In the present work we consider two cases, $\varepsilon = 0.05$ and $\varepsilon = 0.25$, referring to them as weak and moderate driving, respectively. Both these cases are considered in the next section by means of numerical simulation.

3 Numerical simulation

In the present section we study transport properties of cold atoms in a optical potential described in the preceding section. For this purpose, we integrate numerically the Schrödinger equation (1) for the ensemble of 1000 realizations of the potential. The initial condition is chosen in the Gaussian form

$$\Psi(x, t=0) = C \exp \left[-\frac{(x - x_0)^2}{4\sigma_x^2(0)} \right], \quad (19)$$

where $\sigma_x(0) = 10\pi$, $x_0 = 0$, C is the constant determined by the normalization condition

$$\int |\Psi(x)|^2 dx = 1. \quad (20)$$

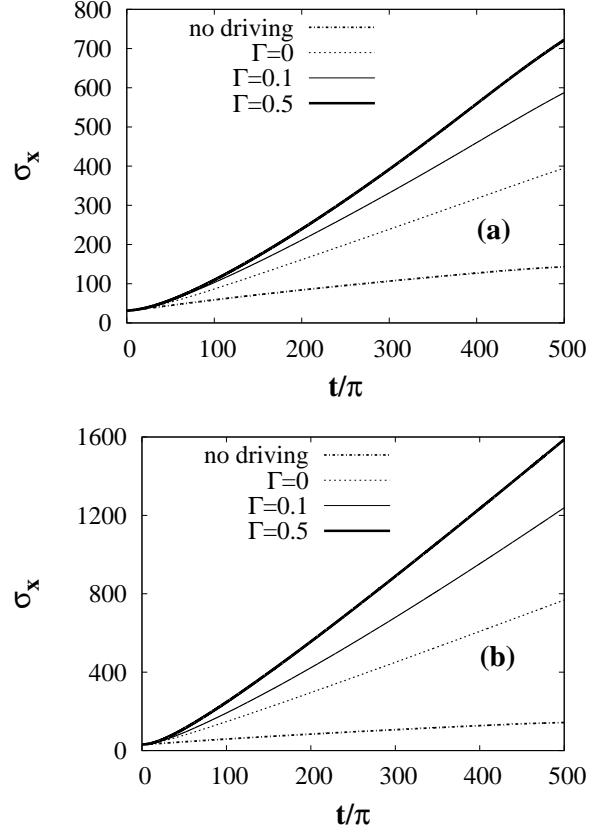


Fig. 4. Ensemble-averaged position variance as function of time. (a) $\varepsilon = 0.05$, (b) $\varepsilon = 0.25$.

3.1 Transport in the case of weak driving: dragging regime

Let's begin the discussion of numerical results corresponding to the case of weak driving $\varepsilon = 0.05$. Fig. 4(a) demonstrates time dependence of ensemble-averaged position variance

$$\sigma_x = \frac{1}{\sqrt{J}} \sqrt{\sum_{j=1}^J (Q_j - r_j^2)}, \quad (21)$$

where $J = 1000$ is the number of potential realizations, r_j is wavepacket displacement calculated with the j th realization of the potential via the formula

$$r_j = \int x |\Psi^{(j)}(x)|^2 dx, \quad (22)$$

and Q_j is squared displacement determined as

$$Q_j = \int x^2 |\Psi^{(j)}(x)|^2 dx. \quad (23)$$

Hereafter $\Psi^{(j)}(x)$ means the solution of the Schrödinger equation (1) with j th realization of the potential. For comparison, the curve corresponding to the case $\varepsilon = 0$ is also plotted. Time-dependent perturbation significantly enhances wavepacket spreading as compared to the undriven case for all values of the noise parameter Γ . Linear

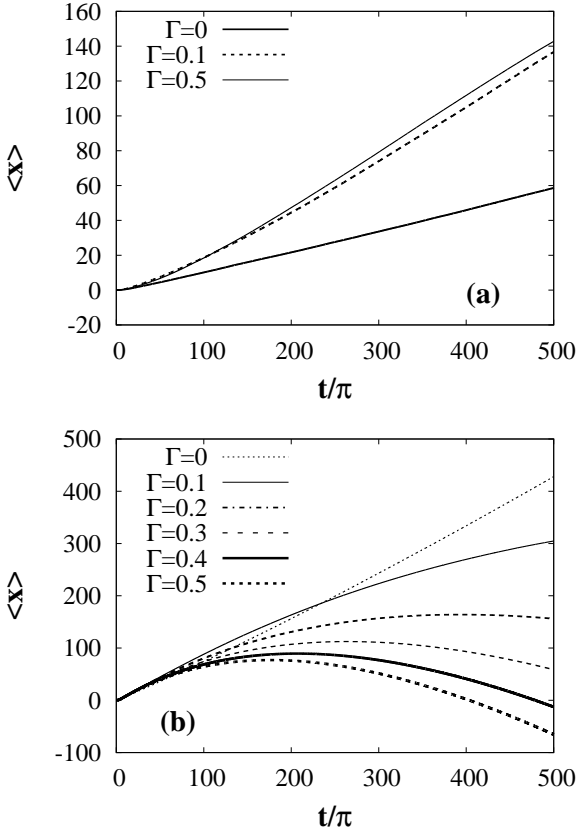


Fig. 5. Mean position as function of time. (a) $\varepsilon = 0.05$, (b) $\varepsilon = 0.25$.

dependence of σ_x on time indicates excitation of ballistic states. The rate of spreading increases with increasing of Γ . So, it turns out that broadening of the perturbation's spectral bandwidth enhances heating of atoms. Fast spreading is accompanied by relatively slow drift of a wavepacket towards $x \rightarrow \infty$, that is, in the same direction as the phase velocity of the perturbation. It is illustrated in Fig. 5 representing time dependence of mean position determined as

$$\langle x \rangle = \frac{1}{J} \sum_j^J r_j. \quad (24)$$

Thus, we observe dragging of atoms by the wave-like perturbation. Notably, directed flux in the presence of noise is much larger than in the purely deterministic case $\Gamma = 0$. It means that noise leads to more extensive transitions between localized and ballistic states. However, the rate of drift is nearly the same for $\Gamma = 0.1$ and $\Gamma = 0.5$, as well as for intermediate values of Γ (not shown). It means that enhancement of heating is compensated by fluctuations of perturbation phase velocity.

It is also informative to consider time dependence of the ensemble averaged spatial population imbalance defined as

$$\langle W \rangle = \frac{1}{J} \sum_{j=1}^J (W_j^+ - W_j^-), \quad (25)$$

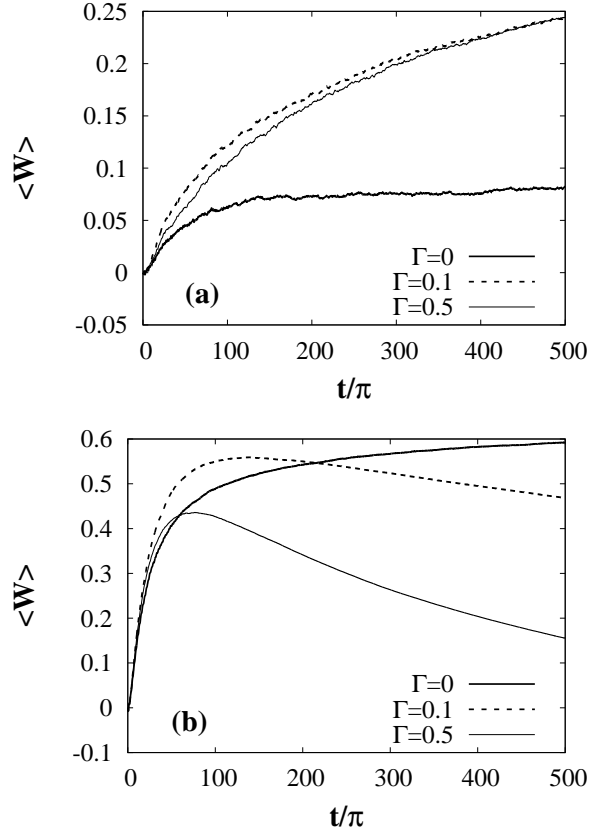


Fig. 6. Ensemble-averaged spatial population imbalance as function of time. (a) $\varepsilon = 0.05$, (b) $\varepsilon = 0.25$.

where

$$\begin{aligned} W_j^+ &= \int_0^\infty |\Psi^{(j)}(x)|^2 dx, \\ W_j^- &= \int_{-\infty}^0 |\Psi^{(j)}(x)|^2 dx. \end{aligned} \quad (26)$$

Figure 6(a) shows that the strongest growth of spatial population imbalance is observed within the initial time period, and then the growth becomes slower, although imbalance remains far from the maximal accessible value 1. The behaviour of $\langle W \rangle(t)$ reflects the process of energy transfer from localized states to ballistic ones having certain momentum value. It turns out that states with both negative and positive momentum values are excited, with relatively small prevalence of the latter ones. As the population of localized states decreases with time, the excitation weakens, and growth of $\langle W \rangle$ becomes slower.

It is important to emphasize that excitation of ballistic states is a stochastic process, therefore, transport properties with some single realization can deviate significantly from the picture drawn by statistical averaging. To illus-

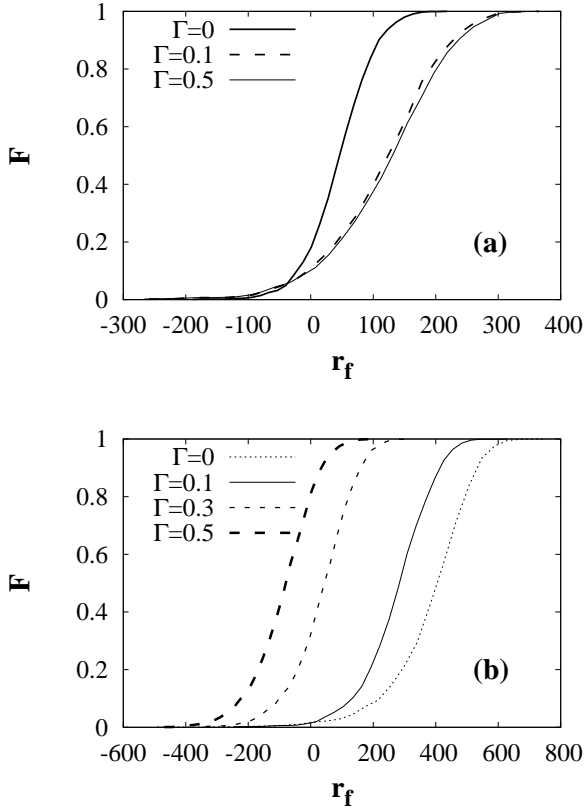


Fig. 7. Cumulative distribution of wavepacket displacements at $t = 500\pi$. (a) $\varepsilon = 0.05$, (b) $\varepsilon = 0.25$.

trate it, we calculate the function

$$F(r_f) = \int_{-\infty}^{r_f} \rho(r') dr', \quad (27)$$

being the cumulative distribution of displacement values at $t = 500\pi$ for an ensemble of potential realizations. Fig. 7(a) shows that nearly 20 percents of realizations exhibit prevalence of transport in the opposite direction to the dragging if $\Gamma = 0$. Increasing of Γ allows one to reduce fraction of such “anomalous” realizations to nearly 10 percents. Thus, onset of directed current with controllable direction is possible only with probability not equal to one.

3.2 Transport in the case of moderate driving: onset of current reversal

Now let's consider the case of the moderate driving, $\varepsilon = 0.25$. According to Fig. 4(b), there is also ballistic spreading of a wavepacket, but the rate of spreading is increased approximately two times as compared with the case of weak driving. As in the case of weak driving, addition of noise remarkably enhances spreading.

Time dependence of mean position looks in qualitatively different way. In the noiseless case $\Gamma = 0$, we observe the same regime of dragging as in the case of weak driving, with significantly increased current velocity. However, as noise is added, the behaviour changes drastically. Codirectional motion with the perturbation persists only until some time horizon, and then current changes direction. It is clearly demonstrated in Fig. 5(b). The time of current reversal decreases with increasing of Γ . Comparing Figs. 5(b) and 6(b), one can deduce that, despite of the current reversal, the majority of atomic states remain in the range of positive values of x , albeit their fraction decreases with time. It means that backward current is produced by progressive accumulation of states with large negative velocity.

Onset of current reversal is also reflected in the distributions of wavepacket displacements at $t = 500\pi$, demonstrated in Fig. 7(b). In the noiseless case $\Gamma = 0$, almost all realizations of potential give rise to positive displacements. Inclusion of fluctuations increases probability of backward displacement. For $\Gamma = 0.5$, backward displacements dominate the overall statistics.

Thus, numerical simulation exhibits a somewhat unusual phenomenon of current reversal occurring if the noise parameter Γ is non-zero. Theoretical explanation of this phenomenon is given in the next section.

4 Dynamics in the momentum space

The origin of the current reversal observed can be found out if we examine wavepacket evolution in the space of momentum eigenstates

$$|m\rangle = \psi_m = \frac{1}{\sqrt{L}} e^{(i/\hbar)(p_m x - E_m t)}, \quad (28)$$

where

$$p_m = \frac{2\pi m}{L}, \quad E_m = \frac{p_m^2}{2M}, \quad (29)$$

$$m = -m_0, -m_0 + 1, \dots, m_0 - 1, m_0.$$

Temporal evolution of occupation probabilities

$$\rho_m = \left| \int \psi_m^* \Psi dx \right|^2 \quad (30)$$

can be described by the master equations [61]

$$\frac{d\rho_l}{dt} = \sum_m G_{lm}(\rho_m - \rho_l), \quad (31)$$

where $G_{mn} = |H_{lm}|^2 \equiv l|\hat{H}|m\rangle$. In our model, the matrix elements H_{lm} responsible for transition between the momentum states can be represented as a sum

$$H_{lm} = H_{lm}^a + H_{lm}^b + H_{lm}^c, \quad (32)$$

where

$$H_{lm}^a = \frac{f(t)e^{i\omega_{lm}t}}{L} \int_0^L e^{i\Delta p_{lm}x/\hbar} \sin x dx, \quad (33)$$

$$H_{lm}^b = \frac{f(t+\tau)e^{i\omega_{lm}t}}{L} \int_0^L e^{i\Delta p_{lm}x/\hbar} \cos x \, dx, \quad (34)$$

$$H_{lm}^c = \frac{e^{i\omega_{lm}t}}{L} \int_0^L U(x) e^{i\Delta p_{lm}x/\hbar} \, dx, \quad (35)$$

$$\Delta p_{lm} = p_l - p_m, \quad \omega_{lm} = (E_l - E_m)/\hbar. \quad (36)$$

After integration, we find

$$H_{lm}^a = \begin{cases} \frac{i \operatorname{sgn}(\Delta p_{lm})}{2} f(t) e^{-i\omega_{lm}t}, & \Delta p_{lm} \pm 1, \\ 0, & \Delta p_{lm} \neq 1 \end{cases} \quad (37)$$

$$H_{lm}^b = \begin{cases} \frac{1}{2} f(t+\tau) e^{-i\omega_{lm}t}, & \Delta p_{lm} \pm 1, \\ 0, & \Delta p_{lm} \neq 1 \end{cases} \quad (38)$$

$$H_{lm}^c = \exp(-i\omega_{lm}t) U_{lm}, \quad (39)$$

Terms H_{lm}^a and H_{lm}^b correspond to resonant transitions between states under action of the time-dependent perturbation $V(x, t)$. It is reasonable to average them over sufficiently long time interval in order to eliminate short-time interference effects. This procedure corresponds to calculation of the transition amplitudes by means of the celebrated Fermi's golden rule. The averaging terms are expressed as

$$H_{lm}^a = \frac{i}{2T} \operatorname{sgn}(\Delta p_{lm}) \int_0^T f(t) \exp(-i\omega_{lm}t) \, dt, \quad (40)$$

$$H_{lm}^b = \frac{1}{2T} \int_0^T f(t+\tau) \exp(-i\omega_{lm}t) \, dt. \quad (41)$$

$f(t)$ and $f(t+\tau)$ can be represented as Fourier integrals

$$f(t) = \frac{1}{2\pi} \int F(\omega) e^{i\omega t} \, d\omega, \quad (42)$$

$$f(t+\tau) = \frac{1}{2\pi} \int F'(\omega) e^{i\omega t} \, d\omega. \quad (43)$$

Substituting (42) and (43) into (40) and (41), and taking the limit $T \rightarrow \infty$, we find

$$H_{lm}^a = \frac{i}{2} \operatorname{sgn}(\Delta p_{lm}) F(\omega = \omega_{lm}), \quad (44)$$

$$H_{lm}^b = \frac{1}{2} F'(\omega = \omega_{lm}/\hbar). \quad (45)$$

Thus, only the resonant contribution is taken into account in these equations. Assuming that time of phase correlations of $f(t)$ is large compared to τ , we can use approximation

$$F'(\omega = \omega_{lm}) \simeq e^{i\omega_{lm}\tau} F(\omega = \omega_{lm}). \quad (46)$$

Validity of this approximation requires that noise bandwidth $\Delta\omega$ should not be large. It is satisfied for moderate values of the noise parameter Γ .

Term H_{lm}^c corresponds to transitions caused by incoherent scattering on the random potential $U(x)$. These transitions lead to broadening of the momentum spectra and remarkably affect wavepacket spreading. However, this term is not resonant, and, after some finite time interval, the transitions it causes weaken due to interference. In addition, the scattering process doesn't influence the directivity of transport because it creates left-going and right-going states with equal probabilities. As the transport directivity is our major concern, we can take into account the effect of broadening by means of proper choice of initial conditions in (31), while the contribution of the term H_{lm}^c into rate constants can be eliminated by means of averaging over time. It implies that qualitative (but not quantitative) description of directed current variability can be obtained in terms of a reduced model that doesn't involve the disordered potential. Thus, the time-averaged matrix element reads

$$\bar{H}_{lm} = F_{\text{res}} \left[\frac{i}{2} \operatorname{sgn}(\Delta p_{lm}) + e^{-i\omega_{lm}\tau} \right], \quad (47)$$

and we can find the corresponding transition rate

$$G_{lm} = \varepsilon^2 S_{\text{res}} \left[\cos^2 \omega_{lm}\tau + \left(\sin \omega_{lm}\tau + \frac{\operatorname{sgn}(\Delta p_{lm})}{2} \right)^2 \right], \quad (48)$$

where $S(\omega)$ is harmonic noise power spectrum given by [57]

$$S(\omega) = \frac{\beta\Gamma}{\pi[\omega^2\Gamma^2 + (\omega^2 - \omega_0^2)^2]}. \quad (49)$$

Formula (48) infers that transitions in the halfspaces corresponding to negative and positive momentum values have different rates. As spectral width of harmonic noise is relatively small, we can approximate ω_{lm} as ω_0 . Then, taking into account (17), one can replace $\omega_{lm}\tau$ as $\operatorname{sgn}(\omega_{lm})\pi/2$ and simplify (48) as

$$G_{lm} \approx \varepsilon^2 S_{\text{res}} \left[\operatorname{sgn}(\omega_{lm}) + \frac{\operatorname{sgn}(\Delta p_{lm})}{2} \right]^2 \quad (50)$$

We have $\operatorname{sgn}(\omega_{lm}) = -\operatorname{sgn}(\Delta p_{lm})$ for left-going states and $\operatorname{sgn}(\omega_{lm}) = \operatorname{sgn}(\Delta p_{lm})$ for right-going ones. This means that transitions between left-going momentum states are much less extensive. Since only limited range of momentum values corresponds to strongly coupled states, there should be accumulation of population inside left-going states which have larger lifetimes.

To verify the above suggestion, we solve numerically the system of master equations (31) with the Gaussian initial condition

$$\rho_m = A \exp\left(-\frac{p_m^2}{2\sigma_p^2}\right), \quad (51)$$

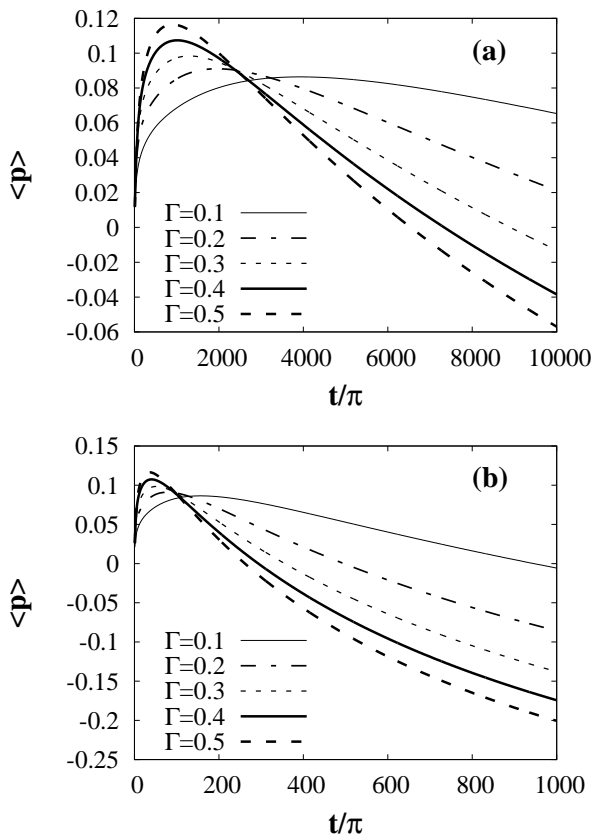


Fig. 8. Mean momentum calculated by solving equations (31) as function of time. (a) $\varepsilon = 0.05$, (b) $\varepsilon = 0.25$.

where

$$A = \frac{1}{\sum_m \rho_m}. \quad (52)$$

We use relatively large momentum variance $\sigma_p = 1$ in order to mimic the effect of scattering on the disorder potential $U(x)$. Fig. 8 represents dependence of mean momentum on time for various values of ε and Γ . Comparison of Figs. 8(a) and (b) reveals evident similarity between the cases of $\varepsilon = 0.05$ and $\varepsilon = 0.25$. Nevertheless, current reversal occurs in the former case on significantly longer timescales. Thus, it turns out that the plane-wave perturbation is able to drag particles only within some limited time intervals before the reversal. Reversals don't appear in data shown in Fig. 5(a) because the time interval considered is too short. Broadening of the perturbation spectrum increases number of efficiently coupled momentum states and results in more extensive diffusion in the momentum space. Consequently, the reversal happens earlier. This explains facilitation of transport with increasing Γ . It should be noted that calculations for longer timescales reveal further reversals, however, time between two successive reversals rapidly grows.

5 Summary

The present work is devoted to a simple one-dimensional quantum model involving a disordered potential and time-dependent perturbation in the form of a fluctuating plane wave. This model can be realized experimentally with optically trapped cold atoms. Also, it can serve as a toy model for studying phonon-induced charge transport in disordered wires.

The main result of the work is the onset current reversals which occur for non-zero values of the model parameter quantifying fluctuations of the time-dependent force. It is shown that this effect is a consequence of diffusion inhomogeneity in the momentum space. Enhancement of noise facilitates diffusion in the momentum space and diminishes the time needed for the reversal onset.

It should be mentioned that influence of the plane-wave-like perturbation onto dynamics of quantum wavepacket was recently considered in [49]. In that paper, it was found that atomic current can change its sign as the perturbation amplitude increases. Despite the results of [49] and this paper look similar, the underlying mechanisms are different. In the model considered in [49], the plane-wave-like perturbation leads to excursion of quasimomentum inside the lowest energy band. In our model, dynamics is not restricted to the lowest band, moreover the crucial role in the reversal onset is played by inter-level transitions accompanied by heating of atoms.

It is important to note that onset of current reversals can be qualitatively described by means of the reduced kinetic model that doesn't take into account effect of the disordered background potential, that is, disorder doesn't play crucial role for the reversals. It means that such reversals can be readily observed in simpler models where potential involves only fluctuating plane wave. We hope to address this issue in forthcoming works. Another issue of interest is how the current reversal effect manifests itself under quantum-to-classical crossover.

Acknowledgments

This work is supported by grants from the Russian Foundation of Basic Research (project 12-02-31416), and the joint grant of the Far-Eastern and Siberian Branches of the Russian Academy of Sciences.

References

1. I. Buluta and F. Nori, *Science* **326**, 108 (2009)
2. A. R. Kolovsky, *Europhys. Lett.* **93**, 20003 (2011)
3. M. Aidelsburger *et al.*, *Phys. Rev. Lett.* **107**, 255301 (2011)
4. M. Aidelsburger *et al.*, *Appl. Phys. B* **113**, 1 (2013)
5. H. Miyake, G. A. Siviloglou, C. J. Kennedy, W. C. Burton, and W. Ketterle, *Phys. Rev. Lett.* **111**, 185302 (2013)
6. D. N. Maksimov, I. Y. Chesnokov, D. V. Makarov, and A. R. Kolovsky, *J. Phys. B: Atomic, Molecular and Optical Physics* **46**, 145302 (2013)

7. G. G. Carlo *et al.*, Phys. Rev. A **74**, 033617 (2006)
8. J. Gong and P. Brumer, Phys. Rev. Lett. **97**, 240602 (2006)
9. S. Denisov, L. Morales-Molina, S. Flach, and P. Hänggi, Phys. Rev. A **75**, 063424 (2007)
10. L. Morales-Molina and S. Flach, New J. Phys. **10**, 013008 (2008)
11. D. Poletti, G. Benenti, G. Casati, P. Hänggi, and B. Li, Phys. Rev. Lett. **102**, 130604 (2009)
12. F. Zhan, S. Denisov, A. V. Ponomarev, and P. Hänggi, Phys. Rev. A **84**, 043617 (2011)
13. V. I. Belinicher and B. I. Sturman, Usp. Fiz. Nauk **130**, 415 (1980)
14. K. N. Alekseev, E. H. Cannon, J. C. McKinney, F. V. Kusmartsev, and D. K. Campbell, Phys. Rev. Lett. **80**, 2669 (1998)
15. M. V. Entin and L. I. Magarill, Phys. Rev. B **73**, 205206 (2006)
16. W. Weber *et al.*, Phys. Rev. B **77**, 245304 (2008)
17. M. A. Pyataev and S. N. Ulyanov, Phys. Rev. B **79**, 235428 (2009)
18. S. A. Tarasenko, Phys. Rev. B **83**, 035313 (2011)
19. Y. Y. Kiselev and L. E. Golub, Phys. Rev. B **84**, 235440 (2011)
20. L. Ermann and D. L. Shepelyansky, Eur. Phys. J. B **79**, 357 (2011)
21. A. V. Nalitov, L. E. Golub, and E. L. Ivchenko, Phys. Rev. B **86**, 115301 (2012)
22. O. Romero-Isart and J. J. García-Ripoll, Phys. Rev. A **76**, 052304 (2007)
23. G. De Chiara *et al.*, Phys. Rev. A **77**, 052333 (2008)
24. M. Holthaus, G. H. Ristow, and D. W. Hone, Phys. Rev. Lett. **75**, 3914 (1995)
25. D. F. Martinez and R. A. Molina, Phys. Rev. B **73**, 073104 (2006)
26. D. F. Martinez and R. A. Molina, Eur. Phys. J. B **52**, 281 (2006)
27. H. Yamada and K. S. Ikeda, Phys. Lett. A **248**, 179 (1998)
28. H. Yamada and K. S. Ikeda, Phys. Rev. E **59**, 5214 (1999)
29. H. Yamada and K. S. Ikeda, Physica B **263264**, 156 (1999)
30. H. Yamada, Physica E **9**, 389 (2001)
31. H. Yamada and K. S. Ikeda, Phys. Rev. E **65**, 046211 (2002)
32. H. Yamada and K. S. Ikeda, Phys. Lett. A **328**, 170 (2004)
33. C. D'Errico *et al.*, New J. Phys. **15**, 045007 (2013)
34. J. M. Moix, M. Khasin, and J. Cao, New J. Phys. **15**, 085010 (2013)
35. M. Wilkinson, J. Phys. A: Math. Gen. **21**, 4021 (1988)
36. M. Wilkinson, J. Phys. A: Math. Gen. **24**, 2615 (1991)
37. D. Makarov and M. Uleysky, JETP Lett. **83**, 522 (2006)
38. D. V. Makarov and M. Y. Uleysky, Phys. Rev. E **75**, 065201 (2007)
39. D. V. Makarov, Tech. Phys. Lett. **34**, 303 (2008)
40. D. V. Makarov, E. V. Sosedko, and M. Y. Uleysky, Eur. Phys. J. B **73**, 571 (2010)
41. D. V. Makarov and L. E. Kon'kov, Phys. Lett. A **377**, 3093 (2013)
42. S. Denisov, S. Flach, and P. Hänggi, Phys. Rep. **538**, 77 (2014)
43. H. Yamada and K. S. Ikeda, Phys. Lett. A **222**, 76 (1996)
44. J. Jiang *et al.*, Phys. Rev. B **72**, 235408 (2005)
45. S. Roche, J. Jiang, L. E. F. F. Torres, and R. Saito, J. Phys.: Cond. Matt. **19**, 183203 (2007)
46. M. T. Greenaway, A. G. Balanov, D. Fowler, A. J. Kent, and T. M. Fromhold, Phys. Rev. B **81**, 235313 (2010)
47. B. A. Glavin, V. A. Kochelap, T. L. Linnik, K. W. Kim, and M. A. Strosio, Phys. Rev. B **65**, 085303 (2002)
48. A. J. Kent *et al.*, Phys. Rev. Lett. **96**, 215504 (2006)
49. M. T. Greenaway, A. G. Balanov, and T. M. Fromhold, Phys. Rev. A **87**, 013411 (2013)
50. D. N. Maksimov and A. F. Sadreev, JETP Lett **86**, 584 (2008)
51. F. M. Izrailev and A. A. Krokhin, Phys. Rev. Lett. **82**, 4062 (1999)
52. U. Sivan and Y. Imry, Phys. Rev. B **35**, 6074 (1987)
53. B. L. Altshuler, I. K. Zarekeshev, S. A. Kotochigova, and B. I. Shklovskii, Sov. Phys. JETP [Zh. Eksp. Teor. Fiz. **94**, 343] **67**, 15 (1988)
54. B. I. Shklovskii, B. Shapiro, B. R. Sears, P. Lambrianides, and H. B. Shore, Phys. Rev. B **47**, 11487 (1993)
55. S. Flach, O. Yevtushenko, and Y. Zolotaryuk, Phys. Rev. Lett. **84**, 2358 (2000)
56. D. Makarov and L. Kon'kov, arXiv preprint arXiv:1406.2427 (2014)
57. A. Neiman and L. Schimansky-Geier, Phys. Rev. Lett. **72**, 2988 (1994)
58. V. S. Anishchenko, A. B. Neiman, F. Moss, and L. Schimansky-Geier, Phys. Usp. **42**, 7 (1999)
59. S. Burkhardt, M. Kraft, R. Mannella, and S. Wimberger, New J. Phys. **15**, 045008 (2013)
60. S. Wimberger, R. Mannella, M. Kraft, and S. Burkhardt, Fluct. Noise Lett. **12**, 1340005 (2013)
61. M. Wilkinson, B. Mehlig, and D. Cohen, Europhys. Lett. **75**, 709 (2006)

